JACS
JOURNAL OF THE AMERICAN CHEMICAL SOCIETY
Article
pubs.acs.org/JACS

Kinetics of Ion Transport in Perovskite Active Layers and Its Implications for Active Layer Stability

Monojit Bag,[†,⊥] Lawrence A. Renna,[†,⊥] Ramesh Y. Adhikari,[‡] Supravat Karak,[†] Feng Liu,[§] Paul M. Lahti,[†] Thomas P. Russell,[§,∥] Mark T. Tuominen,[‡] and D. Venkataraman*[,†]

[†]Department of Chemistry, University of Massachusetts Amherst, Amherst, Massachusetts 01003-9303, United States
[‡]Department of Physics, University of Massachusetts Amherst, Amherst, Massachusetts 01003-9303, United States
[§]Materials Science Division, Lawrence Berkeley National Laboratory, Berkeley, California 94720-1730, United States
[∥]Department of Polymer Science & Engineering, University of Massachusetts, Amherst, Massachusetts 01003-9303, United States

Supporting Information

ABSTRACT: Solar cells fabricated using alkyl ammonium metal halides as light absorbers have the right combination of high power conversion efficiency and ease of fabrication to realize inexpensive but efficient thin film solar cells. However, they degrade under prolonged exposure to sunlight. Herein, we show that this degradation is quasi-reversible, and that it can be greatly lessened by simple modifications of the solar cell operating conditions. We studied perovskite devices using electrochemical impedance spectroscopy (EIS) with methylammonium (MA)-, formamidinium (FA)-, and MA_xFA_{1-x} lead triiodide as active layers. From variable temperature EIS studies, we found that the diffusion coefficient using MA ions was greater than when using FA ions. Structural studies using powder X-ray diffraction (PXRD) show that for $MAPbI_3$ a structural change and lattice expansion occurs at device operating temperatures. On the basis of EIS and PXRD studies, we postulate that in $MAPbI_3$ the predominant mechanism of accelerated device degradation under sunlight involves thermally activated fast ion transport coupled with a lattice-expanding phase transition, both of which are facilitated by absorption of the infrared component of the solar spectrum. Using these findings, we show that the devices show greatly improved operation lifetimes and stability under white-light emitting diodes, or under a solar simulator with an infrared cutoff filter or with cooling.

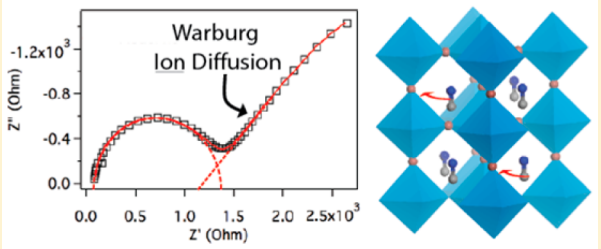

INTRODUCTION

Lead halide-based perovskite solar cells[1−10] have drawn considerable interest because of their high efficiency and low temperature solution processability.[11] But a major practical limitation of these systems is their poor stability under ambient conditions[12,13] and their degradation upon prolonged exposure to heat and sunlight.[14] Previous reports have focused on degradation pathways attributed to moisture and temperature effects.[14−16] But thus far, the origin and nature of *photoinduced* degradation is largely unexplored.

In inorganic−organic hybrid lead iodide perovskites, an organic counterion, typically alkyl ammonium, occupies voids within a 3D framework created by vertex-shared PbI_6 octahedra. Migration of ions within the 3D framework has been speculated to be an important factor leading to device instability and hysteresis in device current−voltage (J−V) profiles.[17] Some reports have explored ionic drift/transport in the perovskite active layer.[18−24] But there is no clear understanding of the factors that facilitate undesired ion transport in the materials. Toward clarifying the possible role of ion transport in the degradation of perovskite solar cells, we studied them in operando, by electrochemical impedance spectroscopy (EIS)[25−27] combined with structural analysis of active layers by powder X-ray diffraction (PXRD), using varied illumination and temperature conditions.

EXPERIMENTAL SECTION

Methylammonium iodide (MAI) was synthesized by the following procediure. Methylamine (24 mL, 33%) was dissolved in EtOH (100 mL) under $Ar_{(g)}$. HI (5 mL, 55%) was added dropwise to the stirred methylamine solution. After ca. 15 min, the solution was concentrated in vacuo. The yellow solid was washed several times with diethyl ether, recrystallized from diethyl ether/EtOH to form a white solid, and then dried in vacuo at 70 °C.

Formamidinium iodide (FAI) was synthesized by the following procedure. Formamidine acetate (2.5 g) was dissolved in EtOH (100 mL) under $Ar_{(g)}$. HI (10.77 mL, 57%) was added dropwise to stirred formamidine acetate solution. After ca. 2 h at ∼50 °C, the solution was concentrated in vacuo. The yellow solid was washed several times with diethyl ether, recrystallized from diethyl ether/EtOH to form a white solid and then dried in vacuo at 70 °C.

Devices were fabricated as follows. ITO substrates (∼20 $\Omega \cdot sq^{-1}$) were cleaned by ultrasonication of the substrates submerged in soap solution, then acetone, and then isopropyl alcohol followed by drying in a hot air oven at 140 °C for 2 h. Poly(3,4-ethylenedioxythio-

Received: August 12, 2015
Published: September 28, 2015

DOI: 10.1021/jacs.5b08535
J. Am. Chem. Soc. 2015, 137, 13130−13137

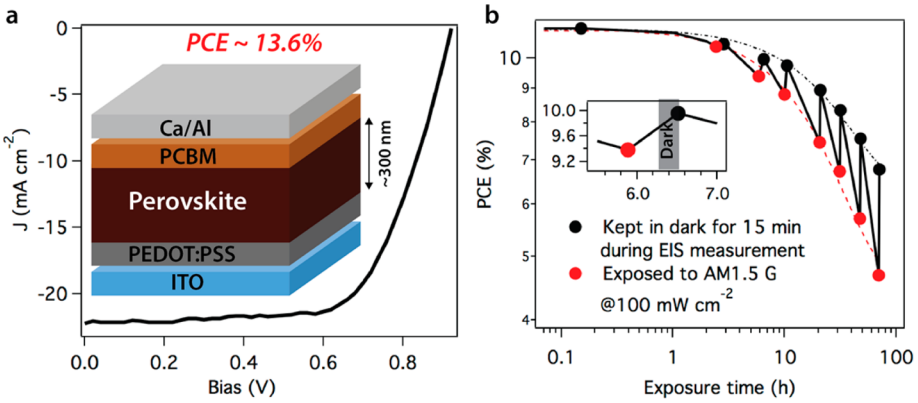

Figure 1. (a) $MAPbI_3$ perovskite solar cell light $J-V$ characteristics for best cell without photomask. Inset: Device architecture. (b) Device efficiency as a function of light exposure time. EIS was carried out at each points represented as red circle. Black circle represents the efficiency just after the device was kept in dark for 15 min during dark impedance measurement.

Table 1. $MAPbI_3$ Perovskite Solar Cell Metrics

device condition	J_{SC} (mA·cm^{-2})	V_{OC} (V)	FF (%)	η (%)	R_s (Ω·cm^2)	R_{sh} (kΩ·cm^2)
Sample 1, as prepared	18.85	0.865	70.2	11.45	5.8	0.857
After 70 h in light	8.66	0.929	58.1	4.68	11.8	0.328
After 15 min in dark	12.67	0.851	62.8	6.78	9.2	0.330
Sample 2, as prepared	17.57	0.983	66.4	11.47	7.5	0.896
After 5 days	17.55	0.970	61.5	10.48	10.6	0.686

phene)−polystyrenesulfonate (PEDOT:PSS) (Clevios PVP AI 4083) was filtered through a 0.45 μm polyvinylidene fluoride (PVDF) filter (Wilkem Scientific), then spin coated onto the substrates at 3000 rpm for 30 s. The PEDOT:PSS coated ITO substrates were then annealed at 140 °C for 20 min in a hot air oven. PbI_2 (40 wt %) was dissolved in dry *N*,*N*-dimethylformamide (DMF) and filtered through a 0.45 μm polytetrafluoroethylene (PTFE) (Wilkem Scientific) filter. The hot solution (~80 °C) was then spin coated at 6000 rpm onto a hot substrate (~80 °C) for 60 s. The PbI_2 coated film was then kept on a hot plate (90 °C) to dry for 1 h. MAI, FAI and mixtures of MAI and FAI (1:1 by wt) were dissolved in isopropyl alcohol (40 mg·mL^{-1}) and spin coated on the PbI_2 coated substrates at 6000 rpm for 60 s at room temperature. $MAPbI_3$ and $MA_xFA_{1-x}PbI_3$ samples were annealed on a hot plate (85 °C) for 1 h. $FAPbI_3$ samples were annealed at 160 °C for 10 min. The devices were then kept in the dark for over 12 h. [6,6]-Phenyl-C_{61}-butyric acid methyl ester (PCBM) in chlorobenzene (20 mg mL^{-1}) as an electron-transporting layer was then spin coated atop the devices at 1000 rpm for 60 s inside a glovebox. Next, a 15 nm thick Ca electrode was thermally deposited at a rate of 0.5 Å·s^{-1} followed by 100 nm of Al electrode deposited at a rate of 1−3 Å·s^{-1}, all at a chamber pressure of 1×10^{-6} mbar.

Current−voltage ($J-V$) curves of the perovskite solar cells were tested under an AM 1.5G solar simulator at 100 mV·cm^{-2} light intensity inside a N_2 filled glovebox, at time intervals over 70 h. Impedance was measured using an Agilent 4294A Precision Impedance Analyzer at different bias voltages after each efficiency measurement, using a frequency analyzer under AM 1.5G simulated illumination, as well as under dark condition. Temperature dependent study was conducted using a thermoelectric heater/cooler with a thermocouple attached to measure in situ temperature. $J-V$ measurements were made without a photomask to compare with EIS experiments were a photomask cannot be used. Device stability experiments were performed using a cool white-LED array (12 V, 10 W) light source and an AM 1.5G solar simulator at 100 mW cm^{-2} light intensity and the same solar simulator with an infrared cutoff, Newport-Oriel KG5 filter.

PXRD measurements were made using samples on cleaned glass slides with a PANalytic X'Pert^3 X-ray diffractometer having a Ni filter, 1/2 in. diverging slit, vertical goniometer, and X'Celerator detector. Measurements were made from $2\theta = 5°-60°$ under Cu Kα (1.542 Å).

RESULTS AND DISCUSSION

$J-V$ curves of planar heterostructure (Figure 1a, inset) perovskite solar cells shown in Figure 1a were measured under inert atmosphere inside a glovebox by scanning the voltage from the short circuit current (J_{SC}) to the open circuit voltage (V_{OC}) at a scan rate of 250 mV·s^{-1}. We obtained an average power conversion efficiency (PCE) of 10.3% over 32 $MAPbI_3$ devices with a maximum PCE of 13.6% (without using a photomask) under an AM 1.5G solar simulator at 100 mW·cm^{-2} light intensity. The average over 32 devices and maximum efficiency obtained using perovskite having *both* counterions ($MA_xFA_{1-x}PbI_3$) was 11.6% and 13.3%, respectively. By comparison, the maximum efficiency obtained from $FAPbI_3$ devices was 8.9%. Low PCE in $FAPbI_3$ devices has been attributed to their weak near-IR absorption.[28] The $J-V$ characteristics, reproducibility, and device crystallinity of these devices are given in Figure S1. For the main discussion below, we focus on results from $MAPbI_3$ and $MA_xFA_{1-x}PbI_3$ devices because of their high PCEs and reproducibility compared to $FAPbI_3$ devices.

Under prolonged illumination, the overall PCE of the devices decreased over time (Figure 1b), with the $MAPbI_3$ devices degrading faster than $MA_xFA_{1-x}PbI_3$ devices. In 20 h, $MAPbI_3$ device PCEs dropped by 40%, whereas the $MA_xFA_{1-x}PbI_3$ device PCEs dropped only by 15% (see Figure S2). Surprisingly, when a previously illuminated $MAPbI_3$ device was kept in the dark for ~15 min and then reilluminated, much of the lost PCE was recovered, indicating that the device degradation was quasi-reversible (Figure 1b). After a period of 70 h in the dark under inert atmosphere inside a glovebox, the PCE of $MAPbI_3$ devices dropped only marginally. Much more impressively, from a similar dark-storage test *for 30 days*, $MA_xFA_{1-x}PbI_3$ device shows *no* appreciable loss in PCE (Figure S4). $MAPbI_3$ devices did show degradation (see Figure S4), which can be attributed to the exposure to light and applied bias when making $J-V$ measurements. Compared to $MAPbI_3$

DOI: 10.1021/jacs.5b08535
J. Am. Chem. Soc. 2015, 137, 13130−13137

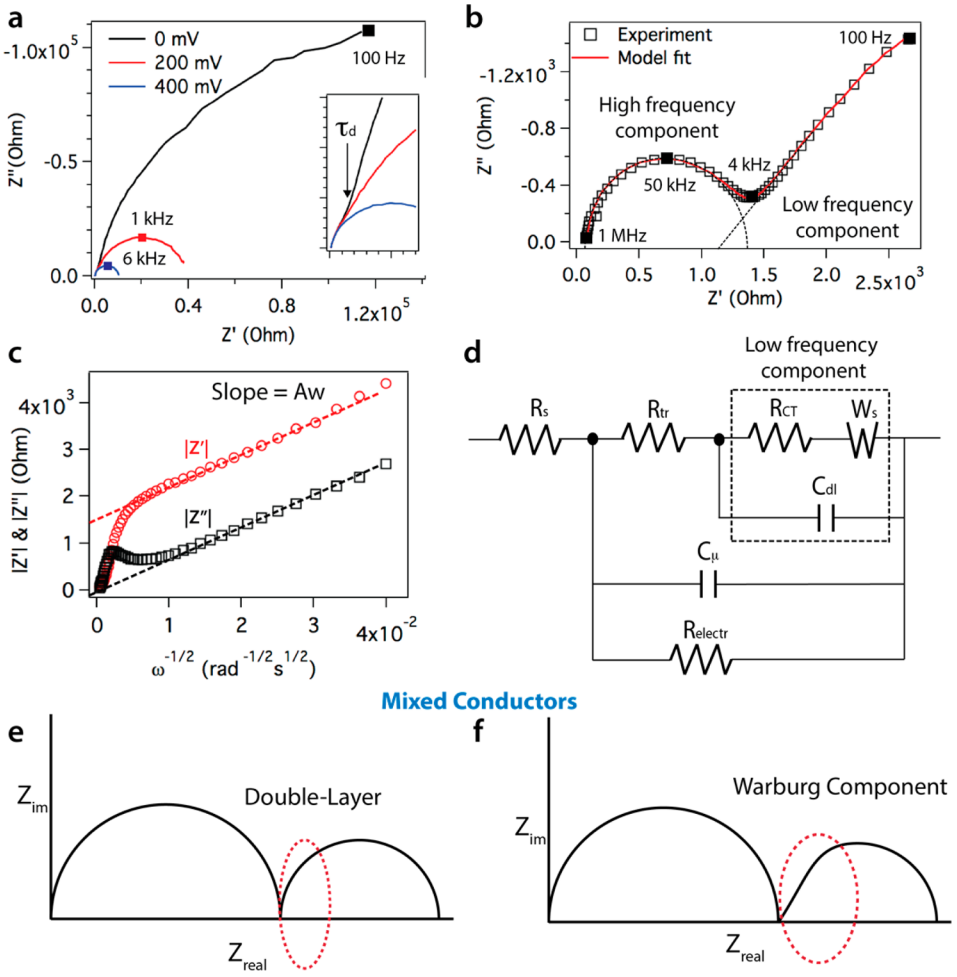

Figure 2. (a) Nyquist plot of $MAPbI_3$ samples under dark. Data was taken from 100 Hz to 1 MHz oscillation frequency at 20 mV AC amplitude and 0 V DC bias. Inset: High frequency component showing transport regime. (b) EIS plot of $MAPbI_3$ sample at 45 °C at 100 mW·cm^{-2} light intensity and 0 V applied bias. (c) Warburg impedance plot of same data. (d) Equivalent circuit diagram of perovskite solar cells showing combined charge and ion transport impedance. (e) Typical Nyquist plot for mixed conductor system with double-layer capacitance showing semicircular feature in low frequency regime. (f) Typical Nyquist plot for mixed conductor system with Warburg diffusion as evidence by the linear portion of the low frequency regime.

devices, we also observed a reduced $J-V$ hysteresis in $MA_xFA_{1-x}PbI_3$ devices (Figure S5). On the basis of these data, we conclude that (a) the device degradation is accelerated by the AM1.5G illumination of the device and *not* by trace oxygen or moisture inside the glovebox (Table 1), and (b) the mixed counterion $MA_xFA_{1-x}PbI_3$ devices exhibit greatly improved stability under dark and under illumination conditions, compared to the corresponding single-counterion devices.

To understand the origin of photoinduced, yet quasi-reversible degradation in the perovskite films, we carried out EIS measurements on devices under dark conditions as well as under AM1.5G illumination in a nitrogen-filled glovebox. In these EIS measurements, the device impedance was measured by applying 20 mV AC voltage whose frequency (ω) is swept from 100 Hz to 1 MHz in 100 equal steps on a logarithmic scale. EIS results are conventionally presented as a Nyquist plot, with the real component of the impedance (Z') as the abscissa and the imaginary part (Z'') as the ordinate.[29] Nyquist plots of a $MAPbI_3$ sample under dark conditions (Figure 2a) versus AM 1.5G solar simulator conditions at 100 mW cm^{-2} light intensity (Figure 2b) show different characteristics. The plots under dark conditions showed a single charge transport regime[29] at low forward bias voltages (V_{app}) with an estimated transit time (τ_d) of ~90 μs (Figure 2a). When V_{app} was increased, a single recombination semicircle was observed, *indicating only one type of charge transport (electronic) is predominant under dark conditions.* The Nyquist plot from a device under illumination shows *two* distinct charge transport regimes, with two semicircles associated with different time constants (τ). The semicircle closest to the origin is associated with the higher frequency spectrum and is attributed predominantly to impedance arising from the electronic transport. The second semicircle is associated with the low frequency spectrum and is attributed to the impedance arising either from charge or mass transfer at the interface or Warburg ion diffusion.[30] Additional data, including light intensity dependence and dark measurements, are shown in Figure S6. As a control experiment, we measured the EIS of a bulk heterojunction organic solar cell having no ions in the active layer, a cell fabricated from poly(3-hexylthiophene) and PCBM. The EIS of this system, as expected, shows only one semicircle in the high frequency regime, under *both* dark and illuminated conditions (Figure S7c,d). On the basis of these results, and

DOI: 10.1021/jacs.5b08535
J. Am. Chem. Soc. 2015, 137, 13130−13137

literature precedent describing the impedance spectroscopy of systems with two types of charge carriers,[31−33] we assert that the low frequency EIS component *arising only in the illuminated* perovskite is predominately associated with the diffusion of ions.

Prior EIS studies of perovskite-based solar cells attribute the low frequency component to double layer capacitance due to charge accumulation at the interface, not to ion migration.[18,34−40] To account for charge accumulation at the interface in these studies, ion migration to the interface can be invoked. But this low frequency component can also arise from ion diffusion or Warburg diffusion. The tell-tale signature of ion/Warburg diffusion is the presence of a linear region as in Figure 2f in the Nyquist plot instead of just a semicircle as in Figure 2e that indicates double-layer capacitance. A close examination of the published EIS spectra from which charge accumulation effects were concluded shows the presence of a linear component in low frequency Nyquist plot region.[41] This feature is just what we obtained in our in operando EIS measurements.

To support our ion diffusion degradation mechanism hypothesis further, we modeled the ionic diffusion in the low frequency regime as a Warburg element (W_S),[42] whose impedance is represented in eq 1:

$$W_S = A_W \frac{\tanh(j\omega T_W)^P}{(j\omega T_W)^P} \quad (1)$$

where A_W is the Warburg impedance, T_W is the Warburg time constant, and exponent P is ∼0.5.[32,43] A detailed explanation of the model derivation is given in the Supporting Information. Plots of $|Z'|$ and $|Z''|$ as functions of $\omega^{-1/2}$ show linear behavior in the low frequency regime, with the slope of both lines being equal to A_W[41] (Figure 2c). The imaginary component line intersects the ordinate at zero. This observation is unequivocal proof that this sort of low frequency component arises from Warburg *ion* diffusion.[42]

To evaluate the kinetics of the photoinduced ion transport, the Nyquist plots were modeled as mixed conductor systems based on the equivalent circuit model in Figure 2d, which contains both high frequency electronic elements and low frequency ionic elements.[30,31] In the model circuit, the high frequency component consists of charge and ion transport resistance (R_{tr}) coupled with interfacial charge transfer resistance (R_{CT}). Any ion accumulation at the interface is modeled as an interfacial Debye-layer capacitance (C_{dl}), while chemical capacitance (C_μ) represents the stored charge in the bulk perovskite layer. Free carrier recombination/transport (electrons and holes both) is modeled using another resistance term (R_{electr}) in parallel with the ion diffusion term. Series resistance (R_s) represents contact resistance arising from the electron and hole transport layers, as well as contributions from the measurement apparatus itself. The details of the modeling are provided in the Supporting Information.

Using ZView version 3.4c (Scribner Associates Inc.), we fit the impedance spectra in Figure 2b and all other Nyquist plots to the circuit model shown in Figure 2d, and obtained R_{tr}, R_{CT}, C_{dl}, C_μ, R_{electr}, R_s, A_w, T_w, and P. From the value of T_W, we calculated the effective chemical diffusion coefficient (D) using the eq 2:

$$D = \frac{L_D^2}{T_W} \quad (2)$$

where L_D is the effective ion diffusion length. In our study, a maximum diffusion length was assumed to be equal to the perovskite film thickness (∼300 nm) measured by profilometry. At the 45 °C (318 K) operating temperature of the device, under AM1.5G illumination, D was calculated to be ∼3.6 × 10^{-12} $cm^2 \cdot s^{-1}$ for $MAPbI_3$, ∼2 × 10^{-12} $cm^2 \cdot s^{-1}$ for $MA_xFA_{1-x}PbI_3$, and ∼3 × 10^{-13} $cm^2 \cdot s^{-1}$ for $FAPbI_3$. The ionic diffusion coefficient follows the order MA > MA_xFA_{1-x} ≫ FA, decreasing with increasing size of the ions and being about an order of magnitude higher for the increased stability MA and mixed counterion materials. While some recently reported studies on $MAPbI_3$ perovskite solar cells conclude that iodide[20,21] anion may be the mobile ion, other studies indicate that alkyl ammonium counterion[22−24] is mobile. Recent first-principles, state-of-the-art computational analysis indicated that the time scale associated with iodide ion mobility is <1 μs, but for methylammonium ions to be tens of milliseconds.[23] Given the fast time scale predicted for iodide transport, evidence of iodide transport in EIS would be hidden under the first semicircle, which is dominated by electronic processes. From our EIS measurements, the time constant associated with the Nyquist semicircle that only appears during illumination is on the order of tens of milliseconds. Moreover, we find that diffusion coefficient obtained in $MAPbI_3$ devices ions is greater than that in $FAPbI_3$ devices. Both these observations are consistent with the computational studies reported by De Angelis and co-workers,[23] with all of these results supporting our hypothesis that the mobile ion in illuminated perovskite solar cells of this type is the alkyl ammonium counterion.

The activation energy (E_a) for ionic diffusion can be calculated by its relationship to T_w shown in eq 3:

$$\frac{1}{T_W} = \frac{kT}{h}\frac{a^2\alpha}{L_D^2}\exp\left(\frac{-E_a}{kT}\right) \quad (3)$$

where a is the lattice parameter for the perovskite, α is the coordination factor, h is Planck's constant.[32] By measuring impedance spectra at various temperatures (Figure S8) and plotting $\ln[1/(T \cdot T_W)]$ vs T^{-1} as shown in Figure 3, we calculated for $MAPbI_3$ that E_a = ∼56 $kJ \cdot mol^{-1}$ (∼0.58 eV) in the low temperature regime (<320 K). Interestingly, De Angelis and co-workers calculated E_a = ∼ 0.5 eV[23] and Tateyama and co-workers calculated E_a = 0.57 eV[24] for MA^+ ion migration in a

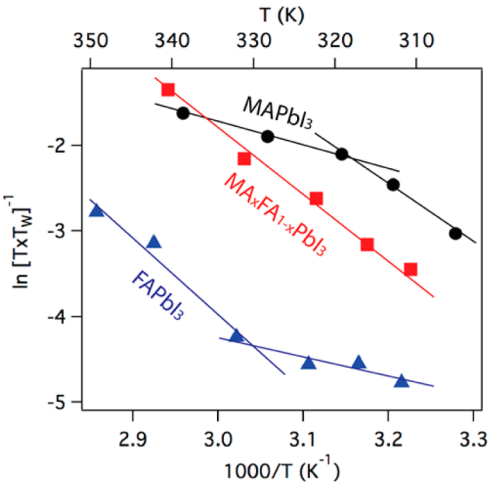

Figure 3. Arrhenius-like plot of $1/(T \cdot T_W)$ vs T^{-1} for $MAPbI_3$, $FAPbI_3$, and $MA_xFA_{1-x}PbI_3$.

DOI: 10.1021/jacs.5b08535
J. Am. Chem. Soc. 2015, 137, 13130−13137

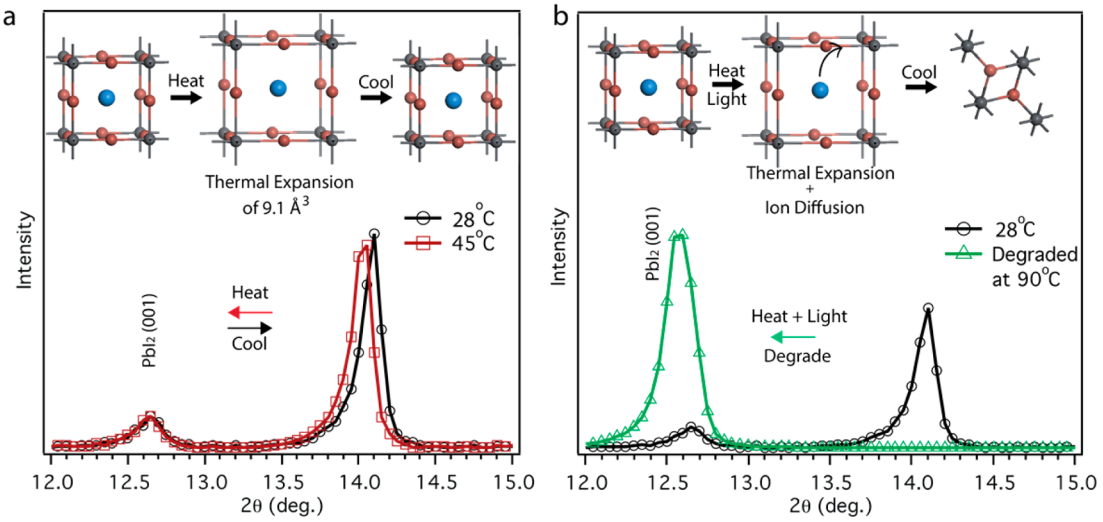

Figure 4. (a) PXRD of $MAPbI_3$ sample at room temperature (28 °C) and after heating with infrared lamp (~45 °C) in dark. The process is reversible once the device gets cooled. (b) PXRD pattern of perovskite sample after prolonged heating in the presence of visible light, showing degradation of perovskite to PbI_2 structure.

tetragonal $MAPbI_3$ supercell. In the high temperature regime (>320 K), we calculate that E_a drops significantly to ~22 kJ·mol^{-1}. We speculate this discontinuity in Arrhenius-like behavior of ionic transport in $MAPbI_3$ arises from a discontinuous volume change induced by a phase transition,[44] as is discussed below. For $MA_xFA_{1-x}PbI_3$, the E_a = ~61 kJ·mol^{-1} was obtained at all temperatures. $MA_xFA_{1-x}PbI_3$ exhibits continuous Arrhenius-like ionic transport because a phase transition does *not* occur as in $MAPbI_3$, again as shown below. The E_a = ~21 kJ·mol^{-1} for $FAPbI_3$ samples at operating temperatures, rising to ~76 kJ·mol^{-1} at higher temperature. These combined results show that under device operating conditions, the activation energy for ion diffusion is higher for MA_xFA_{1-x}, consistent with our observation that devices with mixed ions have a higher stability than those with MA ions alone. $FAPbI_3$ devices also show improved stability (see Figure S4) compared to $MAPbI_3$ devices despite a low E_a; however, the D is also very low, which can explain the enhanced stability.

The temperature dependent ionic conductivity (σ_{ion}) can also be independently obtained from the Warburg impedance (A_W). A plot of $\ln(\sigma_{ion})$ vs $1/T$ and its derivation are shown in Figure S9. Despite varying temperatures from 301 to 353 K, Nyquist plots of devices under dark conditions showed only high frequency charge transport regime behavior (Figure S8d), consistent with electronic-only transport. *No* measurable dark performance ion transport regime was observed, unlike for devices under illumination (Figure S8a–c), indicating that the *ion transport is indeed induced by light.*

To identify the regions in the AM 1.5G solar simulator spectrum that induce the destabilizing ion transport, we first measured EIS for devices operating under a commercial white-LED that does not emit IR or UV components (Figure S10). The EIS Nyquist plots for $MAPbI_3$ devices comparing white-LED versus AM1.5G illuminated performance at 79 mW·cm^{-2} light intensity show significant decrease in the low frequency ion-transport regime under white-LED illumination, indicating slower ion transport compared to the device illuminated by the solar simulator (Figure S11). The ion diffusion coefficient under white-LED was 1.4 × 10^{-12} cm^2·s^{-1}, compared to 3 × 10^{-12} cm^2·s^{-1} under AM1.5G solar simulation. This difference in the diffusion coefficient is consistent with differences in the operating temperatures of the devices, 301 K under LED and 320 K under AM1.5G solar simulator. It further indicates that the ion transport is induced and accelerated *by visible light*: the IR illumination component seems to contribute only to thermal activation of the visible-light induced ion transport.

Grazing incidence wide-angle X-ray scattering (GIWAXS) indicates that all the perovskite films in this study are polycrystalline (Figure S12). We therefore examined perovskite samples (glass/PEDOT:PSS/perovskite/PCBM) by powder X-ray diffraction (PXRD) under different light and temperature conditions, to gauge the effects of visible versus IR illumination components. The PXRD of $MAPbI_3$ device after solar simulator illumination for 15 min showed an increase in lattice dimensions (Figure S13). No such structural lattice change was observed when the sample was exposed to white-LED light alone at a measured operating temperature of 28 °C (301 K). A similar lattice expansion to that induced under AM1.5G solar simulator illumination was also observed for illumination with an IR-only source (150 W commercial IR lamp), as shown in Figure 4a. The tetragonal ($I4cm$) $MAPbI_3$ perovskite (211) PXRD peak[44] at 2θ = 23.48° actually disappears as the temperature rises above 45 °C (see Figure S14), while peaks showing a transition to cubic perovskite ($Pm3m$) are observed. However, this transition reverses when the IR lamp is switched off. PXRD of both $MA_xFA_{1-x}PbI_3$ and $FAPbI_3$ show the PXRD peaks of a trigonal ($P3m1$) structure at 45 °C, consistent with the literature.[45] These show no phase transitions, but they do show an increase in lattice parameters with IR illumination, similar to $MAPbI_3$.

To extract lattice parameters and unit cell volumes before and after heating, the PXRD data was refined using the Rietveld method using known structures[46,47] as starting points. Upon heating with the IR lamp (~45 °C, 318 K), the volume change observed in $MAPbI_3$ was 9.1 Å^3 per unit cell, a 3.66% relative expansion. These observations indicate reversible perovskite lattice expansion under IR heating that correlates with the quasi-reversible thermal/IR PCE cycling that we observed in these solar cells (Figure 1b). The volume increase that accompanies the tetragonal to cubic structural phase change in $MAPbI_3$ has been reported to occur discontinuously,[44] which also correlates with the ion transport activation energy barrier

DOI: 10.1021/jacs.5b08535
J. Am. Chem. Soc. 2015, 137, 13130–13137

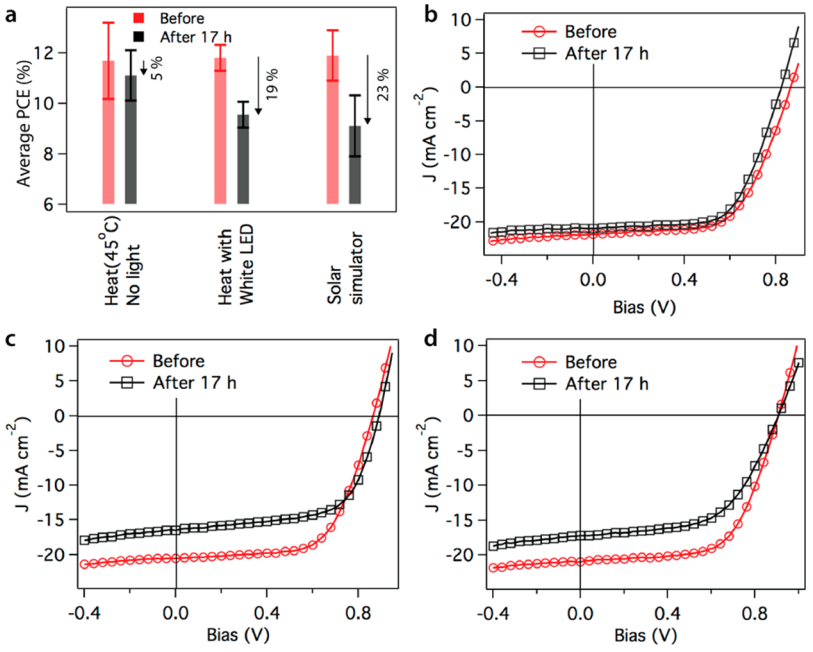

Figure 5. (a) Mixed counterions perovskite solar cell stability after 17 h continually under dark at 45 °C, white-LED light at 45 °C, and AM1.5G solar simulator at 100 mW·cm^{-2} light intensity. *J*−*V* curves averaged over 4 devices before and after (b) heating in dark at 45 °C, (c) heating at 45 °C under white-LED, and (d) AM1.5G solar simulator.

discontinuity from 56 to 22 kJ·mol^{-1} that we find at ∼320 K. The PXRD analyses for $MA_xFA_{1-x}PbI_3$ and $FAPbI_3$ indicate 4.6 and 2.2 Å^3 per unit cell volume increases upon heating, which are relative expansions of 0.63% and 0.23%, respectively (Figure S15). $MA_xFA_{1-x}PbI_3$ does *not* undergo a structural phase transition, and its thermal expansion is quite low compared to that of $MAPbI_3$; thus, ionic diffusion in this mixed system follows continuous Arrhenius behavior. There was no observed phase change for $FAPbI_3$, nor is there any literature evidence of structural changes at high temperatures, so the increase in E_a observed for $FAPbI_3$ samples requires further investigation.

The EIS and PXRD results correlated with device performance in this study provide a comprehensive and revised picture of the origin of the photoinduced degradation of perovskites. The EIS studies show that that ion diffusion is associated with the degradation, and that the diffusion is light induced and thermally activated, and that the alkyl ammonium-type counterions are the diffusion ions. PXRD proves that the perovskite lattices expand on heating, but that this process is reversible. There is a strong correlation between the ionic diffusion coefficient and the activation energy barrier for ion transport with device stability. In $MAPbI_3$, lower activation energy barrier coupled with a higher diffusion coefficient of ions leads to poor device stability under light and dark. Moreover, the $MAPbI_3$ activation energy decreases at high temperature, further promoting ion transport. By contrast, in mixed $MA_xFA_{1-x}PbI_3$ devices, a higher activation energy barrier coupled with the lower diffusion coefficient of ions leads to a better stability under light and dark. This last finding has important practical consequences in the search for more stable perovskite solar cell formulations.

Since the ion diffusion is light induced but thermally activated, we hypothesized that the device stability would be further increased if the devices were operated under conditions that do not increase the device temperature. Indeed, with $MA_xFA_{1-x}PbI_3$, the PCE under white-LED light (*sans* IR component) illumination was stable over the full 20 h duration of an experiment, as shown in Figure 5 and Figure S2. The device stability was also vastly improved when a KG5 filter was used to block the near-IR component of the AM1.5G illuminator. Finally, the device was also stable under standard AM 1.5G illumination when the device was air-cooled with a fan (Figure 6). Devices kept at 45 °C for 17 h under dark

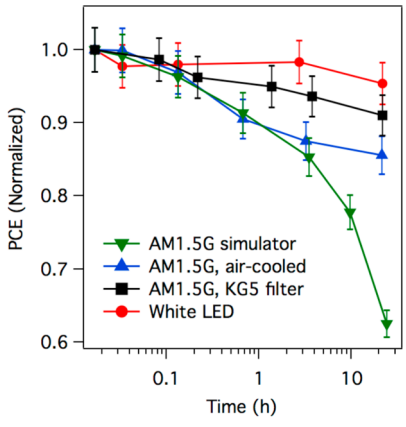

Figure 6. $MAPbI_3$ perovskite device stability (normalized PCE) under AM1.5G solar simulator at 79 mW·cm^{-2} and under AM1.5G solar simulator at 100 mW·cm^{-2} light intensity with a KG5 IR cutoff filter, AM1.5G solar simulator with a fan cooler, and white-LED at 20 mW·cm^{-2}. Three percent error is accounted for *J*−*V* measurement hysteresis and lamp power fluctuation.

showed a 5% decrease in PCE when reilluminated with an AM 1.5G illuminator. After 17 h at 45 °C, PCE of devices showed a 19% decrease under white-LED light and a 23% decrease with AM1.5G solar simulator (Figure 5a). All the device *J*−*V* characteristics were averaged over 4 samples and are shown in Figure 5b−d. These results conclusively show that *a combination of heat and light facilitates rapid ion diffusion and*

DOI: 10.1021/jacs.5b08535
J. Am. Chem. Soc. 2015, 137, 13130−13137

device degradation. The enhanced stability under white LED along with the decrease in ion diffusion coefficient (vide supra) indicates that perovskite active layer degradation is indeed correlated with alkyl ammonium transport. This may be due to accumulation of vacancies, which may destabilize the lattice, and causes collapse to PbI_2.

CONCLUSION

If perovskite-based photovoltaics are truly the future of cheap and efficient solar energy, they cannot degrade under sunlight. It is therefore imperative to develop a fundamental understanding of the light induced degradation pathways in perovskite active layers so that this problem can be solved. In this article, we have clarified the degradation mechanism of alkyl ammonium lead triiodide-based perovskite solar cells under continuous photoillumination. We find that the degradation of perovskite solar cells under sunlight requires *both* an IR and a visible component of the solar spectrum. Further, the quasi-reversibility of the photoinduced degradation phenomenon is observed for the first time in these systems. EIS measurements provide evidence of fast ion transport of the ammonium counterions in the perovskite thin film, which for $MAPbI_3$ can be facilitated by lattice expansion accompanied by a phase transition under simulated solar spectrum containing infrared component. Thus, the photostability can be improved by reducing the infrared component incident on the perovskite solar cells. Mixing a larger counterion (FA) with MA provides the right balance between device performance and stability by circumventing the phase change and increasing the activation energy barrier for ion transport.

ASSOCIATED CONTENT

Supporting Information

The Supporting Information is available free of charge on the ACS Publications website at DOI: 10.1021/jacs.5b08535.

Additional details on device performance and stability, AFM, EIS measurements and modeling, XRD, and GIWAXS (PDF)

AUTHOR INFORMATION

Corresponding Author

*dv@umass.edu

Author Contributions

⊥M.B. and L.A.R. contributed equally.

Notes

The authors declare no competing financial interest.

ACKNOWLEDGMENTS

This work was supported as part of Polymer-Based Materials for Harvesting Solar Energy (PHaSE), an Energy Frontier Research Center funded by the U.S. Department of Energy, Office of Science, Basic Energy Sciences under Award No. DE-SC0001087. We would like to thank Dr. Akshay Kokil (UMass Lowell) for assistance with device preparation.

REFERENCES

(1) Burschka, J.; Pellet, N.; Moon, S.-J.; Humphry-Baker, R.; Gao, P.; Nazeeruddin, M. K.; Grätzel, M. *Nature* **2013**, *499*, 316.

(2) Etgar, L.; Gao, P.; Xue, Z.; Peng, Q.; Chandiran, A. K.; Liu, B.; Nazeeruddin, M. K.; Grätzel, M. *J. Am. Chem. Soc.* **2012**, *134*, 17396.

(3) Green, M. A.; Ho-Baillie, A.; Snaith, H. J. *Nat. Photonics* **2014**, *8*, 506.

(4) Heo, J. H.; Im, S. H.; Noh, J. H.; Mandal, T. N.; Lim, C.-S.; Chang, J. A.; Lee, Y. H.; Kim, H.-j.; Sarkar, A.; Nazeeruddin, M. K.; Grätzel, M.; Seok, S. I. *Nat. Photonics* **2013**, *7*, 486.

(5) Jeon, N. J.; Noh, J. H.; Kim, Y. C.; Yang, W. S.; Ryu, S.; Seok, S. I. *Nat. Mater.* **2014**, *13*, 897.

(6) Lee, M. M.; Teuscher, J. l.; Miyasaka, T.; Murakami, T. N.; Snaith, H. J. *Science* **2012**, *338*, 643.

(7) Liu, M.; Johnston, M. B.; Snaith, H. J. *Nature* **2013**, *501*, 395.

(8) McGehee, M. D. *Nat. Mater.* **2014**, *13*, 845.

(9) Snaith, H. J. *J. Phys. Chem. Lett.* **2013**, *4*, 3623.

(10) Zhou, H.; Chen, Q.; Li, G.; Luo, S.; Song, T.-b.; Duan, H.-S.; Hong, Z.; You, J.; Liu, Y.; Yang, Y. *Science* **2014**, *345*, 542.

(11) You, J.; Hong, Z.; Yang, Y.; Chen, Q.; Cai, M.; Song, T.-B.; Chen, C.-C.; Lu, S.; Liu, Y.; Zhou, H. *ACS Nano* **2014**, *8*, 1674.

(12) Grätzel, M. *Nat. Mater.* **2014**, *13*, 838.

(13) Niu, G.; Guo, X.; Wang, L. *J. Mater. Chem. A* **2015**, *3*, 8970.

(14) Misra, R. K.; Aharon, S.; Li, B.; Mogilyansky, D.; Visoly-Fisher, I.; Etgar, L.; Katz, E. A. *J. Phys. Chem. Lett.* **2015**, *6*, 326.

(15) Christians, J. A.; Miranda Herrera, P. A.; Kamat, P. V. *J. Am. Chem. Soc.* **2015**, *137*, 1530.

(16) Yang, J.; Siempelkamp, B. D.; Liu, D.; Kelly, T. L. *ACS Nano* **2015**, *9*, 1955.

(17) Unger, E. L.; Hoke, E. T.; Bailie, C. D.; Nguyen, W. H.; Bowring, A. R.; Heumuller, T.; Christoforo, M. G.; McGehee, M. D. *Energy Environ. Sci.* **2014**, *7*, 3690.

(18) Dualeh, A.; Moehl, T.; Tétreault, N.; Teuscher, J.; Gao, P.; Nazeeruddin, M. K.; Grätzel, M. *ACS Nano* **2014**, *8*, 362.

(19) Tress, W.; Marinova, N.; Moehl, T.; Zakeeruddin, S. M.; Nazeeruddin, M. K.; Grätzel, M. *Energy Environ. Sci.* **2015**, *8*, 995.

(20) Eames, C.; Frost, J. M.; Barnes, P. R. F.; O'Regan, B. C.; Walsh, A.; Islam, M. S. *Nat. Commun.* **2015**, *6*, 7497.

(21) Yang, T.-Y. Y.; Gregori, G.; Pellet, N.; Grätzel, M.; Maier, J. *Angew. Chem., Int. Ed.* **2015**, *54*, 7905.

(22) Xiao, Z.; Yuan, Y.; Shao, Y.; Wang, Q.; Dong, Q.; Bi, C.; Sharma, P.; Gruverman, A.; Huang, J. *Nat. Mater.* **2015**, *14*, 193.

(23) Azpiroz, J. M.; Mosconi, E.; Bisquert, J.; De Angelis, F. *Energy Environ. Sci.* **2015**, *8*, 2118.

(24) Haruyama, J.; Sodeyama, K.; Han, L.; Tateyama, Y. *J. Am. Chem. Soc.* **2015**, *137*, 10048.

(25) Freger, V.; Bason, S. *J. Membr. Sci.* **2007**, *302*, 1.

(26) Zhuang, Q.-C.; Wei, T.; Du, L.-L.; Cui, Y.-L.; Fang, L.; Sun, S.-G. *J. Phys. Chem. C* **2010**, *114*, 8614.

(27) Li, M.; Pietrowski, M. J.; De Souza, R. A.; Zhang, H.; Reaney, I. M.; Cook, S. N.; Kilner, J. A.; Sinclair, D. C. *Nat. Mater.* **2014**, *13*, 31.

(28) Hu, M.; Liu, L.; Mei, A.; Yang, Y.; Liu, T.; Han, H. *J. Mater. Chem. A* **2014**, *2*, 17115.

(29) Bisquert, J.; Mora-Sero, I.; Fabregat-Santiago, F. *ChemElectroChem* **2014**, *1*, 289.

(30) Jamnik, J.; Maier, J. *J. Electrochem. Soc.* **1999**, *146*, 4183.

(31) Lai, W.; Haile, S. M. *J. Am. Ceram. Soc.* **2005**, *88*, 2979.

(32) Jasinski, P.; Petrovsky, V.; Suzuki, T.; Anderson, H. U. *J. Electrochem. Soc.* **2005**, *152*, J27.

(33) Javier, A. E.; Patel, S. N.; Hallinan, D. T.; Srinivasan, V.; Balsara, N. P. *Angew. Chem., Int. Ed.* **2011**, *50*, 9848.

(34) Pascoe, A. R.; Duffy, N. W.; Scully, A. D.; Huang, F.; Cheng, Y.-B. *J. Phys. Chem. C* **2015**, *119*, 4444.

(35) Juarez-Perez, E. J.; Wußler, M.; Fabregat-Santiago, F.; Lakus-Wollny, K.; Mankel, E.; Mayer, T.; Jaegermann, W.; Mora-Sero, I. *J. Phys. Chem. Lett.* **2014**, *5*, 680.

(36) Pockett, A.; Eperon, G. E.; Peltola, T.; Snaith, H. J.; Walker, A.; Peter, L. M.; Cameron, P. J. *J. Phys. Chem. C* **2015**, *119*, 3456.

(37) Shao, Y.; Xiao, Z.; Bi, C.; Yuan, Y.; Huang, J. *Nat. Commun.* **2014**, *5*, 5784.

(38) Almora, O.; Zarazua, I.; Mas-Marza, E.; Mora-Sero, I.; Bisquert, J.; Garcia-Belmonte, G. *J. Phys. Chem. Lett.* **2015**, *6*, 1645.

(39) Kim, H. S.; Mora-Sero, I.; Gonzalez-Pedro, V.; Fabregat-Santiago, F.; Juarez-Perez, E. J.; Park, N. G.; Bisquert, J. *Nat. Commun.* **2013**, *4*, 2242.

DOI: 10.1021/jacs.5b08535
J. Am. Chem. Soc. 2015, 137, 13130−13137

(40) Christians, J. A.; Fung, R. C.; Kamat, P. V. *J. Am. Chem. Soc.* **2014**, *136*, 758.
(41) For example in Figure 3b,c of ref 34, we can see Warburg-like linear component in the low frequency regime. However, the equivalent circuit shown in Figure 3a of this reference does not include Warburg component.
(42) Ho, C.; Raistrick, I. D.; Huggins, R. A. *J. Electrochem. Soc.* **1980**, *127*, 343.
(43) Sugimoto, W.; Iwata, H.; Yokoshima, K.; Murakami, Y.; Takasu, Y. *J. Phys. Chem. B* **2005**, *109*, 7330.
(44) Baikie, T.; Fang, Y.; Kadro, J. M.; Schreyer, M.; Wei, F.; Mhaisalkar, S. G.; Grätzel, M.; White, T. J. *J. Mater. Chem. A* **2013**, *1*, 5628.
(45) Binek, A.; Hanusch, F. C.; Docampo, P.; Bein, T. *J. Phys. Chem. Lett.* **2015**, *6*, 1249.
(46) Stoumpos, C. C.; Malliakas, C. D.; Kanatzidis, M. G. *Inorg. Chem.* **2013**, *52*, 9019.
(47) Mashiyama, H.; Kurihara, Y.; Azetsu, T. *J. Korean Phys. Soc.* **1998**, *32*, S156.

DOI: 10.1021/jacs.5b08535
J. Am. Chem. Soc. 2015, 137, 13130−13137